J Mater Sci (2008) 43:6337–6343
DOI 10.1007/s10853-008-2912-7

Effect of gradient composite structure in cofired bilayer composites of $Pb(Zr_{0.56}Ti_{0.44})O_3$–$Ni_{0.6}Zn_{0.2}Cu_{0.2}Fe_2O_4$ system on magnetoelectric coefficient

Rashed Adnan Islam · Chuan-bing Rong · J. P. Liu · Shashank Priya

Received: 25 December 2007 / Accepted: 28 July 2008 / Published online: 16 August 2008

Abstract This study investigates the ferroelectric, ferromagnetic, and magnetoelectric properties of the cofired bilayer composites consisting of piezoelectric phase with formulation 0.9 $Pb(Zr_{0.56}Ti_{0.44})O_3$–0.1 $Pb[(Zn_{0.8/3}Ni_{0.2/3})Nb_{2/3}]$ + 2 (mol%) MnO_2 and 40 mol% ferrite phase with formulation $Ni_{0.6}Zn_{0.2}Cu_{0.2}Fe_2O_4$ (NCZF). A bulk composite of the same composition was also synthesized for comparison. Scanning electron microscope (SEM) investigation using quadrant back scattering detector (QBSD) shows migration of ferrite phases through the interface and energy dispersive X-ray spectroscopy (EDX) analysis with X-ray mapping clarifying these as Cu-rich phases. Improved piezoelectric ($d_{33} \sim 80$ pC/N), ferroelectric (polarization of 60 μC/cm^2 and 0.1% strain), higher magnetization (25 emu/g) and lower coercive field (2.8 Oe) were recorded for bilayer composite. The results indicate that the gradient bilayer composites with tailored composition such that the fraction of the secondary phase is higher may lead to better magnetoelectric material.

R. A. Islam (✉)
Material Science and Engineering, University of Texas at Arlington, 500 West 1st Street, Room # 325 Woolf Hall, Arlington, TX 76019, USA
e-mail: rashed_ms@yahoo.com

C. Rong · J. P. Liu
Department of Physics, University of Texas at Arlington, Arlington, TX 76019, USA

S. Priya
Material Science and Engineering, Virginia Tech, Blacksburg, VA 24061, USA

Introduction

Magnetoelectric (ME) materials posses two or more ferroic properties like polarization, magnetization, or strain as a result of electric field, magnetic field, and stress [1–4]. The interrelation between ferroelectricity and magnetism allows magnetic control of ferroelectric properties and vice versa. Recently, laminated ME composites synthesized by using piezoelectric and magnetostrictive materials have gained attention because they exhibit superior ME response [5–13]. The laminates are generally fabricated by sandwiching and bonding piezoelectric plate/disk/fibers between two layers of magnetostrictive plates/disks/foils [10–13]. In order to fabricate miniature sensors, the approach based on cofiring is more attractive similar to that of multilayer ceramic capacitors. Srinivasan's group has conducted several studies on the multilayers of piezoelectric–ferrite system and shown the promising results for ME response. However, the ME response still remains weaker than that desired for practical applications. Further progress in tailoring the ME properties of the layered composites can be obtained by understanding the microstructural changes in the vicinity of the interface and by quantifying the effect of dopants. In this study, we investigate these two factors for the cofired $Pb(Zr,Ti)O_3$–$Ni_{0.8}Zn_{0.2}Fe_2O_4$ bilayer composites.

The challenge in the synthesis of $Pb(Zr,Ti)O_3$ based cofired bilayer composites utilizing $(Ni,Zn)Fe_2O_4$ as ferromagnetic phase is the mismatch in sintering temperature and shrinkage rate which results in delamination. The addition of CuO to $(Ni,Zn)Fe_2O_4$ helps in reducing the sintering temperature by forming a liquid phase in early stages of sintering which dissolves in the matrix at the later stage [14]. Further, Cu-doped $(Ni,Zn)Fe_2O_4$ has been found to exhibit large grain size and higher density [15, 16].

Thus, 20 mol% CuO-doped (Ni,Zn)Fe_2O_4 was selected as the ferromagnetic phase. For piezoelectric phase, hard PZT of the composition 0.98 [0.9 Pb $(Zr_{0.56}Ti_{0.44})O_3$–0.1 $Pb(Zn_{0.8/3}Ni_{0.2/3})Nb_{2/3}$] + 0.02 MnO_2 [PZT (hard)] was selected since this formulation has been shown to provide high piezoelectric voltage constant of 83 × 10^{-3} V m/N [17].

Experimental

Reagent-grade powders of PbO, ZrO_2, TiO_2, ZnO, NiO, Nb_2O_5, CuO, and Fe_2O_3 were obtained from Alfa Aesar, Co., MA, USA. Stoichiometric ratios of the powders were mixed according to formulation 0.9 $Pb(Zr_{0.56}Ti_{0.44})O_3$–0.1 $Pb[(Zn_{0.8/3}Ni_{0.2/3})Nb_{2/3}]$ + 2 (mol%) MnO_2 (PZT) and $Ni_{0.6}Zn_{0.2}Cu_{0.2}Fe_2O_4$ (NCZF) and ball-milled separately for 24 h with alcohol and YSZ grinding media (5 mm diameter, Tosoh Co., Tokyo, Japan). After drying at 80 °C, the powders were calcined differently. PZT powders were calcined at 800 °C for 3 h and NCZF powders were calcined at 750 °C for 5 h in separate alumina crucibles. Calcined powders were crushed and sieved using a sieve of US mesh #270. X-ray diffraction pattern of all different powders (PZT and NCZF) were taken to check the formation of single phase perovskite (for PZT) or spinel (for NCZF) using Siemens Krystalloflex 810 D500 X-ray diffractometer. For the bilayer composite, first PZT powders were pressed under 5 MPa pressure and the NCZF powders were added on top of PZT powders and pressed under 15 MPa pressure. Mole percentage was calculated from the weight of powder added. Similar composition (40 mol% NCZF) powders were mixed stoichiometrically with alcohol and grinding media in a polyethylene jar and ball milled for 36 h. The slurries were dried at 80 °C, crushed and sieved with a stainless steel sieve of US mesh #170. The powders were then pressed to pellets of size 12.7 × 1.5 mm^2 in a hardened steel die using a hydraulic press under a pressure of 15 MPa. The pellets (both bulk and bilayer) were sealed in a vacuum bag and pressed isostatically in a laboratory cold isostatic press (CIP) under a pressure of 207 MPa. Pressureless sintering of composites was performed in air using a Lindberg BlueM furnace at 1000 °C for 3 h. For bilayer composite, before the final sintering at 1000 °C, the composites were annealed at 950 °C for 1 h and then slowly reached to 1000 °C.

Microstructural analysis of the sintered samples was done by Zeiss Leo Smart SEM using the polished and thermal etched samples. In order to perform ME and dielectric measurements, an Ag/Pd electrode was applied on the samples and fired at 850 °C for 1 h. The samples were poled in silicone bath at 120 °C under a field of 2.5–3 kV/mm for 20 min. Dielectric constant as a function of temperature was measured by using HP 4274A LCR meter (Hewlett Packard Co., USA). The magnetization measurements were carried out with an alternating gradient magnetometer (AGM) up to 1.4 T. High-temperature thermomagnetic curves were measured in a high-temperature oven in a quantum design physical property measurement system (PPMS).

The ME coefficient (dE/dH) was measured by applying an AC magnetic field of 1 Oe amplitude (H) at 1 kHz. The AC magnetic field was generated by a Helmholtz coil powered by Agilent 3320 function generator. The output voltage generated from the composite was measured in a SRS DSP lock-in amplifier (model SR 830). The ME coefficient (mV/cm Oe) was calculated by dividing the output voltage by the applied AC magnetic field and the thickness. The ME coefficient was measured as a function of DC magnetic bias field. For frequency dependence of ME coefficient, the Helmholtz coil was powered by the abovementioned function generator from 1 kHz to 10 MHz and the output voltage was recorded by lock-in amplifier.

Results and discussion

Figure 1a shows the high-magnification interface microstructure of cofired bilayer composite observed using Zeiss Leo Smart SEM on the polished and thermal etched samples. The PZT grain size in the vicinity of the interface was larger than the grains far away from the interface. Liquid phase sintering was found to occur in the PZT phase near the interface which may be associated to the diffusion of Cu at the interface and formation of low melting temperature phase. A low magnification microstructure of the interface showed the presence of porosity along the interface. Far from the interface, the microstructure was found to be dense on both sides. Figure 1b shows the microstructure of the bulk composite synthesized for the comparison purposes under similar sintering conditions. PZT grain size observed in the bulk composite was in the range of 400–500 nm and the NCZF grains were in the range of 200–300 nm. The microstructure was dense with density higher than 98%.

Using scanning electron microscope (SEM) Inlens detector, it was found that there is columnar grain growth in PZT phase as shown in Fig. 2a, which indicates the presence of the liquid phase. Energy dispersive X-ray spectroscopy (EDX) analysis of this region shows significant concentration of Cu atoms and by using SEM quadrant back scattering detector (QBSD) it was found that Cu rich phases have diffused through the interface from NCZF side to the PZT side as shown in Fig. 2b. Near the interface there is a thin region where the presence of ferrite clusters is observed. As the distance from the interface increases

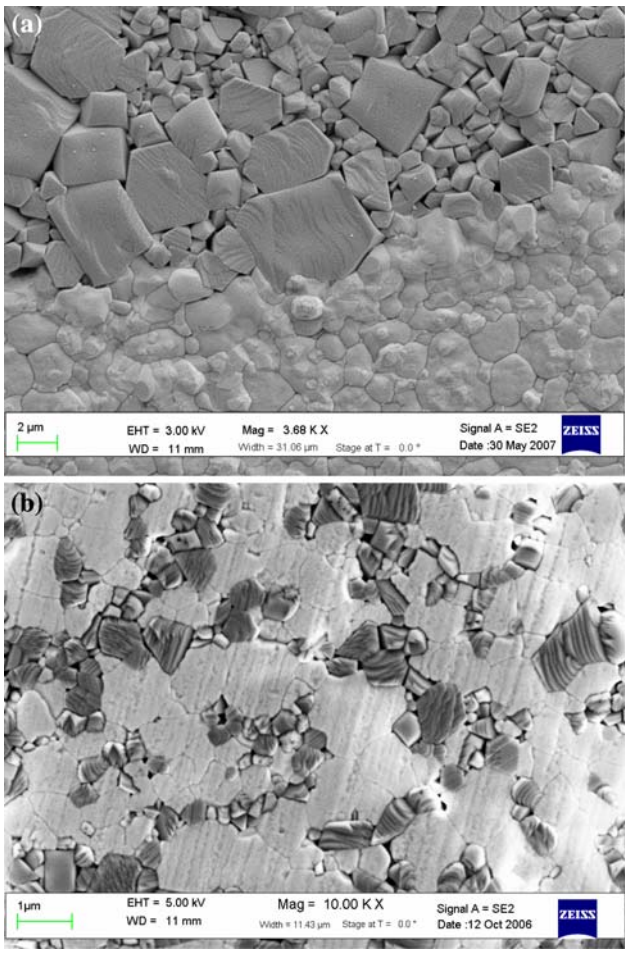

Fig. 1 Microstructure of bilayer and bulk composites: (**a**) bilayer composite and (**b**) bulk particulate composite

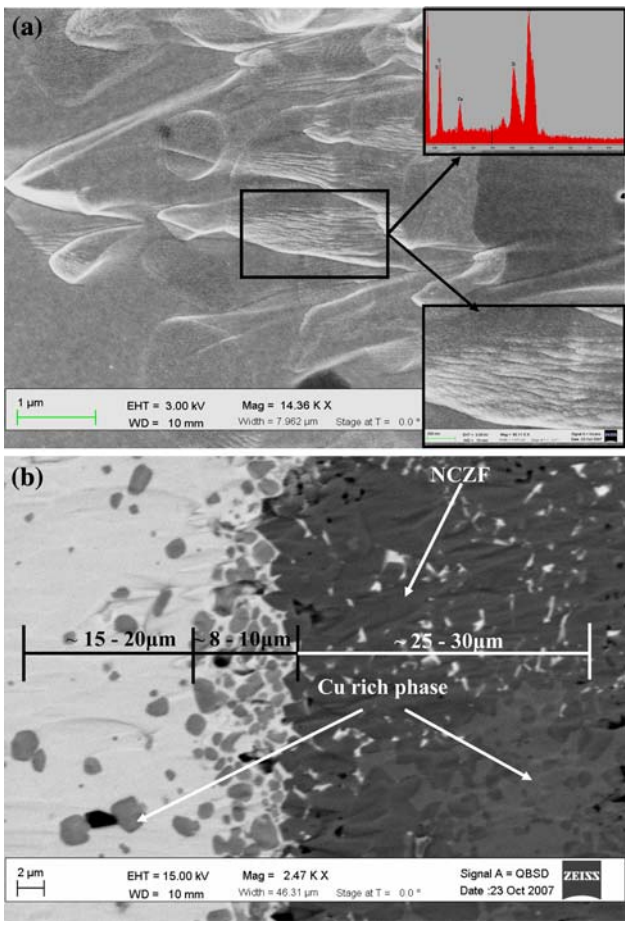

Fig. 2 Microstructure of bilayer bulk composites using (**a**) Inlens detector (inset: magnified view and EDS pattern) and (**b**) quadrant back scattering detector

toward PZT layer, the concentration of ferrite particles decreases, which is expected. Careful observation revealed a contrast in ferrite layer near the interface, which, when investigated by point EDX, indicated that the light contrast is Cu-rich phase whereas the dark contrast is the NCZF. Based on these results it is hypothesized that there is a finite concentration of Cu-rich phase formed near the interface.

An SEM elemental mapping of Pb, Zr, Ni, Fe, and Cu was conducted near the bilayer interface as shown in Fig. 3a. The interface was found to exhibit sharp concentration gradients with slight diffusion of Pb in NCZF phase and Ni in PZT phase. Increased concentration of Cu was found in the PZT phase close to interface which may be responsible for the liquid phase sintering. This Cu may be present as Cu_2O/CuO or $CuFe_2O_4$. X-ray elemental mapping of Cu atoms showed that the region with light contrast is rich in Cu as observed in Fig. 3. The phase diagram for Cu_2O/CuO and PbO shows that there is a eutectic point around 1008 K (735 °C) [18, 19]. Thus the presence of excess PbO and CuO/Cu_2O can produce liquid phase. Figure 1a shows the evidence for the liquid phase sintering. We can also hypothesize that CuO/Cu_2O reacts with the Fe_2O_3 to form non-stoichiometric $CuFe_2O_4$, as it is possible that this reaction occurs in Fe_2O_3-rich environment [20]. Based on Figs. 2 and 3 we can propose that at the interface there is presence of PbO–CuO/Cu_2O eutectic phase and non-stoichiometric $CuFe_2O_4$, which forms a gradient structure given by PZT-PZN/Cu-ferrite/NCZF. Careful investigation of Fig. 2b shows that the migration of the ferrite into PZT–PZN occurs over a distance of 25–30 µm. The 8–10 µm thickness layer adjacent to the interface has high concentration of Cu-rich phase. We estimate the overall thickness of the interface layer as ~50 µm. Next, we try to understand the effect of this gradient structure on the ferroelectric, ferromagnetic, and ME properties.

Figure 4a shows the ferroelectric properties of the cofired bilayer composite. High polarization of 60 µC/cm^2 and strain of 0.1% was recorded at an applied electric field of 4.5 kV/mm. The longitudinal piezoelectric constant, d_{33}, was measured using Berlincourt meter and was found to be

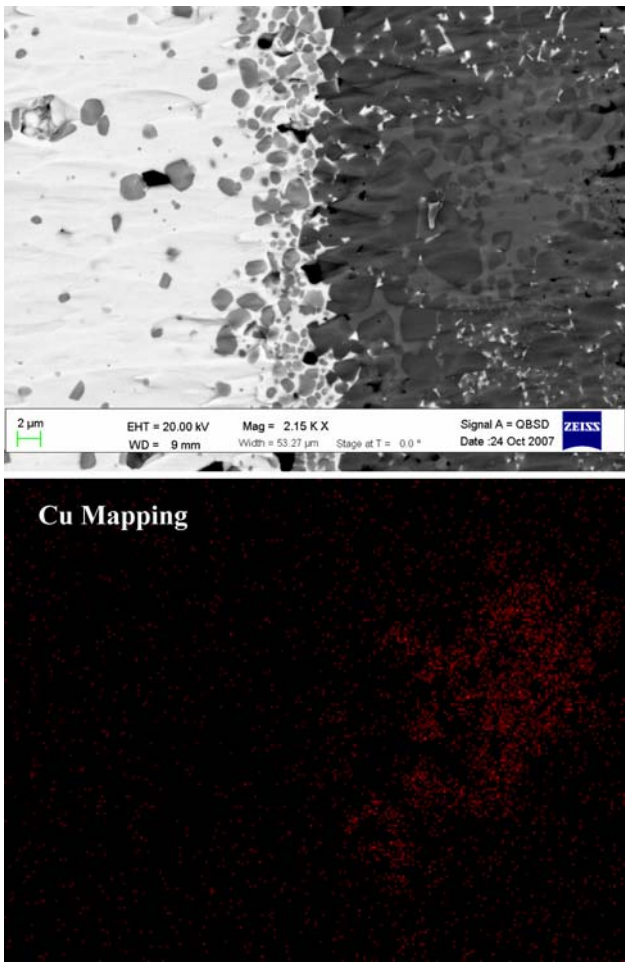

Fig. 3 Cu elemental mapping in the vicinity of the interface

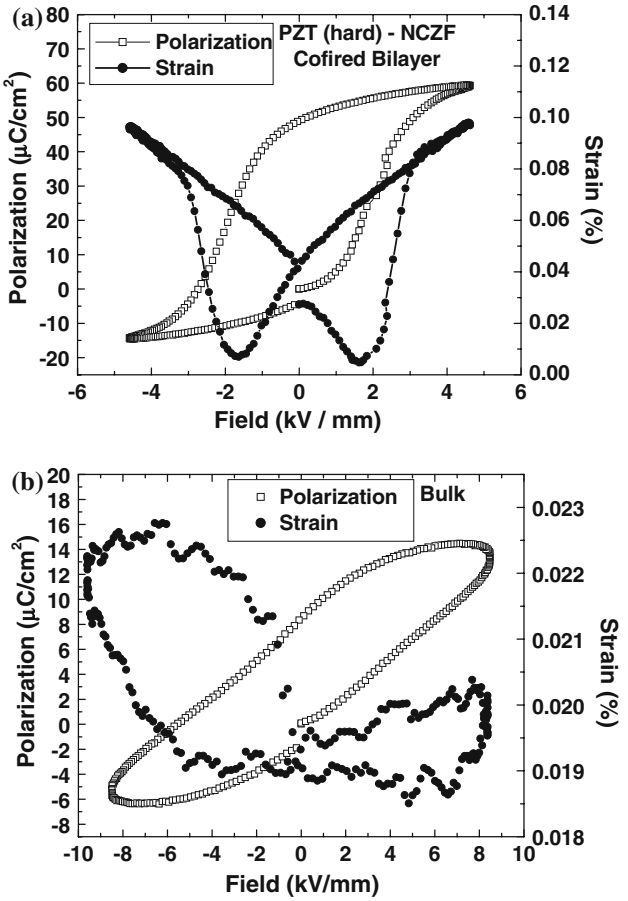

Fig. 4 Ferroelectric loop of PZT–NCZF composite: (**a**) cofired bilayer composite and (**b**) bulk composite

of the order 80 pC/N. The P–E loop for the bulk particulate composite was significantly weak compared to the bilayer, as shown in Fig. 4b. The edges of the loop near the saturation voltage were rounded, which signifies the drop in resistivity. This is expected due to the high concentration of the Cu. The saturation polarization of 16 $\mu C/cm^2$ and strain of 0.022% was recorded at high electric field of 8 kV/mm. The d_{33} magnitude was also found to be very low for the particulate sintered composite of the order of 25–27 pC/N. The results clearly show that the gradient structure in bilayer does results in improved ferroelectric and piezoelectric properties. In order to further elucidate the effect of the gradient structure, we measured the dielectric and magnetic properties which could show if there is any change occurring in the phase symmetry or if there is any averaging of properties.

Figure 5a and b compares the dielectric constant and dielectric loss of the bulk and bilayer composites over a wide range of temperature. The ferroelectric Curie temperature for the bilayer composite was found to be ~355 °C, which is higher than that for bulk composites ~325 °C. (*Note*: The data here are shown at 1 kHz, which indicates high losses at high temperature due to space charge polarization.) A notable distinction in the dielectric response can be seen in the temperature range of 200–225 °C where bilayer composite exhibits a secondary peak. To confirm this result, the test was repeated three times with three different samples and every time the peak was observed. Inset compares the dielectric response of Mn-modified PZT–$NiFe_2O_4$ and PZT–$Ni_{0.7}Zn_{0.3}Fe_2O_4$ bilayers with that of the PZT–PZN–NCZF. It can be noted that the PZT–ferrite bilayers without CuO did not show the secondary peak in dielectric spectra. The dielectric loss behavior of the bilayer composite also exhibited secondary peak at the temperature of ~160 °C. Figure 5c compares the dielectric constant versus temperature of bilayer composite at different frequencies. At 0.1 and 1 kHz, the secondary peak was clearly visible. At 10 kHz a minute slope change was observed. The high loss for cofired bilayer composite is due to the NCZF layer. High loss may hinder the sensitivity of this bilayer composite in real-life application. But the loss can be reduced if the

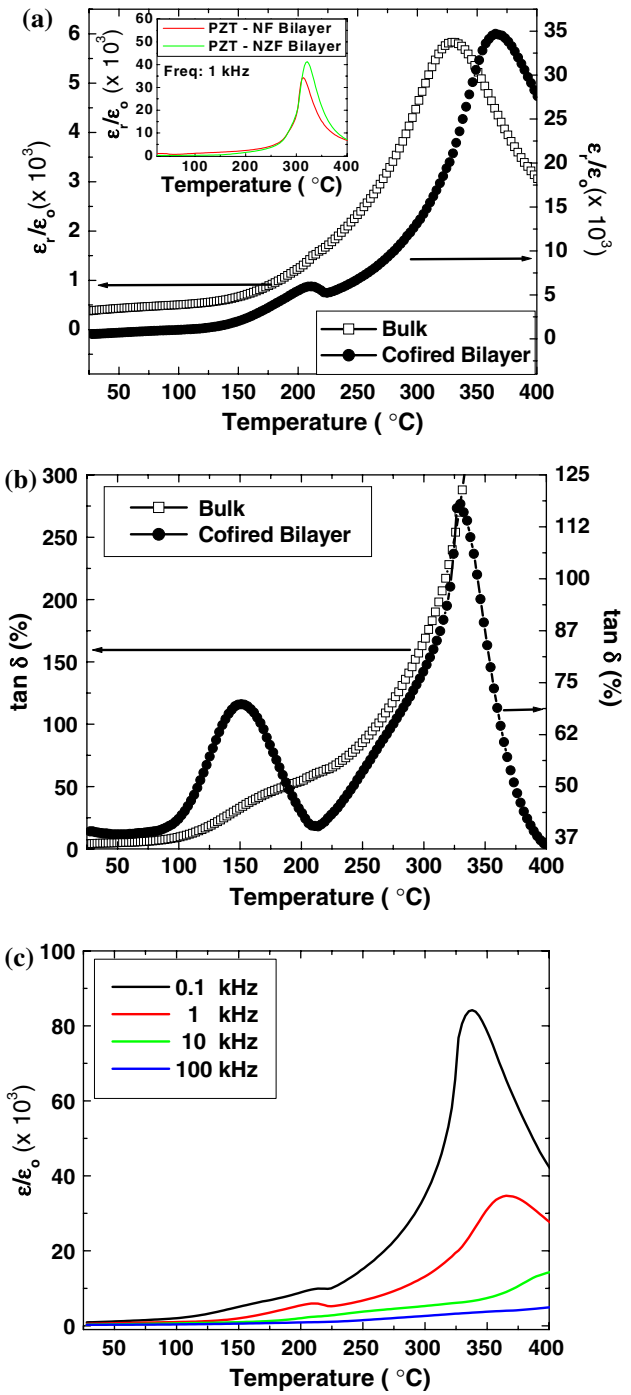

Fig. 5 Dielectric properties of bulk and bilayer as a function of temperature: (**a**) dielectric constant (inset: dielectric constant vs. temperature of PZT–NF and PZT–NZF bilayer), (**b**) dielectric loss, and (**c**) dielectric constant of cofired bilayer as a function of temperature at different frequencies

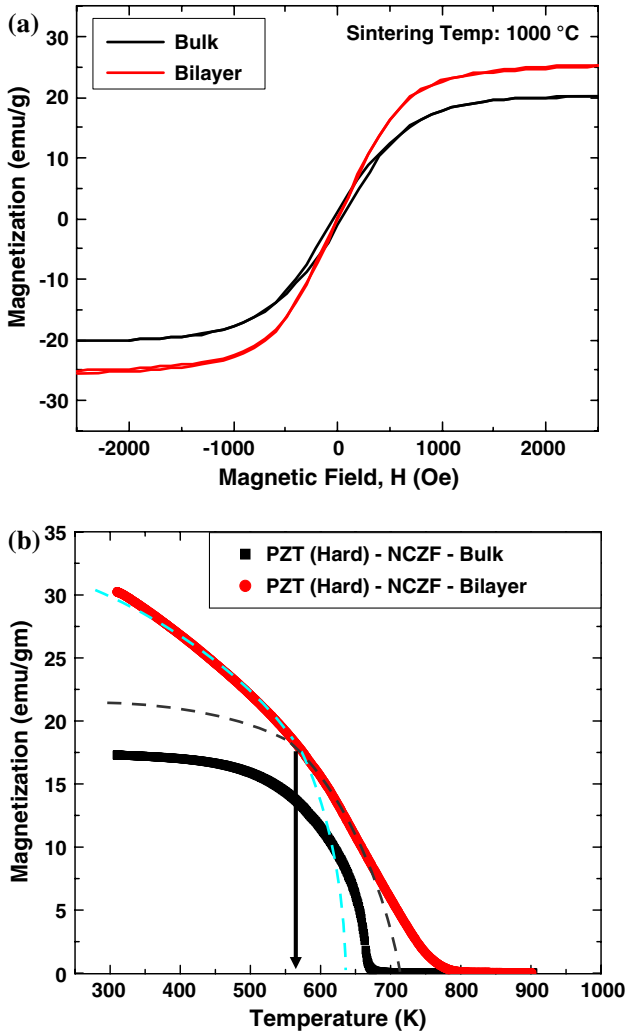

Fig. 6 Ferromagnetic property of two types of composite: (**a**) moment versus field (hysteresis loop) and (**b**) magnetization as a function of temperature

piezoelectric layer is poled individually by inserting an interface electrode layer.

Figure 6a compares the magnetization–magnetic field hysteresis curve of bilayer and bulk composites measured with an AGM up to 1.4 T. It was found that the saturation magnetization (M_s) is higher in bilayer composite than the bulk and the coercivity (H_c) drops from 43 Oe to a very low magnitude of 2.8 Oe. Figure 6b shows the temperature dependence of magnetization for bilayer and bulk composites measured in a high-temperature oven installed with quantum design PPMS. The magnetic Curie temperature (T_C) was determined from the intersection of extrapolations of the greatest slope and flat region above T_C. It was found that T_C of the bilayer composite is higher than that of bulk composite. It can be noticed from Fig. 6b that the magnetization-temperature behavior of the bilayers shows a change in slope at 530 K (~257 °C). This temperature range is similar to where peak in the dielectric behavior was observed, as shown in Fig. 5a.

The results of Figs. 5 and 6 together indicate the presence of secondary phase in the bilayer composites which is reflected both in dielectric and magnetic properties. This

transition could be related to the presence of Cu_2O/CuO or a second ferromagnetic phase evolving from $CuFe_2O_4$ which forms a gradient composite structure with the PZT. Shrotri et al. have shown that doping above 20 mol% Cu in $(Ni,Zn)Fe_2O_4$ makes it unstable and at first CuO starts to form followed by a secondary phase corresponding to the formulation $CuFe_2O_4$ [21, 22]. The free CuO, if present on the piezoelectric side, will react with the PZT–PZN to form low-temperature melting composition which is commonly observed in the low-temperature sintering of ceramics. CuO is a common liquid phase sintering agent in that case. The composite of this low-temperature melting phase and $CuFe_2O_4$ phase may be associated with the transitions observed in the PZT–NCZF composites, though more careful studies using high-temperature X-ray diffraction are required to confirm this hypothesis. The magnetization versus temperature behavior for bilayer composites can be resolved as summation of two curves, as shown by different colored dashed line in Fig. 6b. $CuFe_2O_4$ has a Curie temperature of 743 K [23] and the dashed line (dark blue) indicates the Curie temperature of around 720–730 K. The second line (light blue) corresponds to the $(Ni,Zn)Fe_2O_4$, which has a Curie temperature of about ~640 K. This value approximately corresponds to the Curie temperature of $Ni_{0.65}Zn_{0.35}Fe_2O_4$ [24]. Thus, the overall magnetic response is average of the individual contributions from $CuFe_2O_4$ and $Ni_{0.65}Zn_{0.35}Fe_2O_4$ proportional to the volume fraction.

Figure 7a compares the ME coefficient of Mn-modified PZT–NCZF bilayer and bulk composite. The bilayer composite shows much higher ME coefficient of ~200 mV/cm Oe, whereas the ME coefficient of bulk particulate composite is around 120 mV/cm Oe. The DC bias field at which the composites show maximum ME coefficient is in the range of 900–1200 Oe. This value corresponds to the saturation magnetostriction value of the NCZF phase. The reason behind higher ME coefficient can be attributed to better piezoelectric (d_{33}), ferroelectric polarization, and magnetization of the bilayers. Further, bilayer composites have smaller coercivity as compared to bulk. We also think that the gradient structure obtained in this particular system ($PZT–PZN/CuFe_2O_4/Ni_{0.65}Zn_{0.35}Fe_2O_4$) plays role in the higher ME response. The gradient structure reduces the mismatch in the mechanical impedance which facilitates the strain transfer. Further, it influences the magnitude of the magnetostrictive strain. One way to further enhance the magnitude of the ME coefficient will be to allow the formation of the higher volume fraction magnetostrictive phase at the interface. This could reduce the defects at the interface layer and further enhance the coupling. This may also increase the magnitude of dielectric constant at the room temperature which will result in higher ME coefficient. Figure 7b shows the frequency dependence of ME

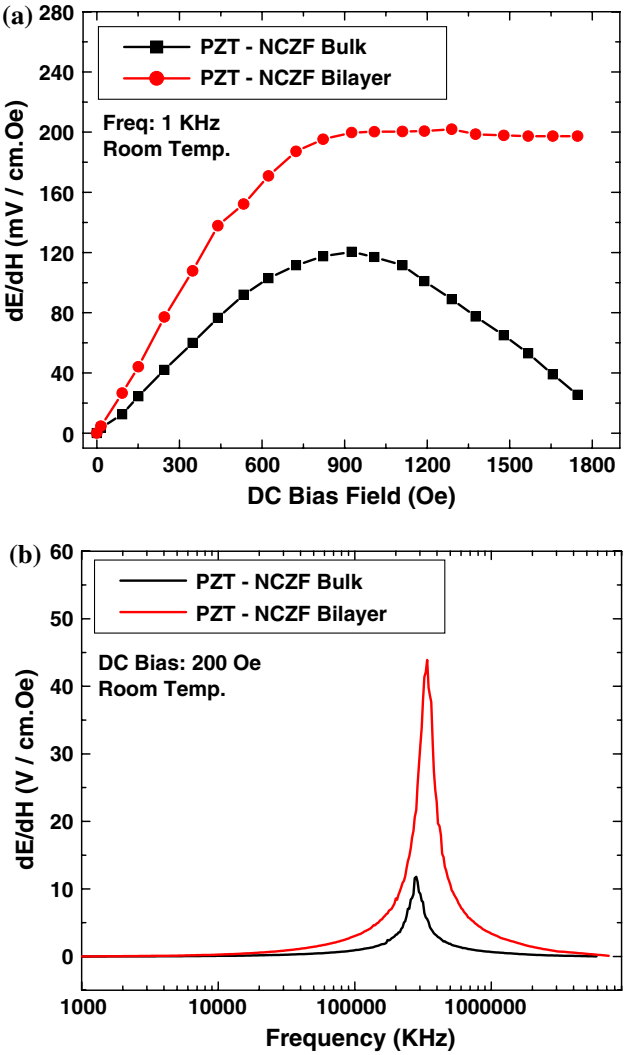

Fig. 7 ME coefficient of PZT–NCZF bilayer and bulk composite: (**a**) ME coefficient as a function of DC bias in T–T mode and (**b**) ME coefficient as a function of frequency

coefficient under a 200 Oe DC field. It was found that at resonance frequency in the range of 200–300 kHz, both the composites show a sharp peak in ME coefficient. The bulk composite shows maximum response of 11 V/cm Oe, whereas bilayer exhibits 43 V/cm Oe.

Conclusion

A detailed comparison between PZT–CuO modified ferrite based cofired bilayer and bulk composite was conducted in order to enhance the ME properties in the sintered composites. It was found that the CuO results in the formation of the secondary $CuFe_2O_4$ phase at the interface which changes the dielectric and magnetic characteristics. The formation of secondary phase enhances the Curie temperature and saturation magnetization, which contributes to the enhanced ME coefficient.

Acknowledgements The authors thank the Department of Energy and Army Research Office for supporting this research. The author (S.P.) also thanks D. Viehland for helpful discussion.

References

1. Wang J, Zheng H, Lofland SE, Ma Z, Ardabili LM, Zhao T et al (2004) Science 303:661. doi:10.1126/science.1094207
2. Ederer C, Spaldin N (2004) Nat Mater 3:849. doi:10.1038/nmat1265
3. Eerenstein W, Mathur ND, Scott JF (2006) Nature 442:759. doi:10.1038/nature05023
4. Hur N, Park S, Sharma PA, Ahn JS, Guha S, Cheong SW (2004) Nature 429:392. doi:10.1038/nature02572
5. Ryu J, Priya S, Uchino K, Viehland D, Kim H (2002) J Korean Ceram Soc 39:813
6. Ryu J, Priya S, Uchino K, Kim H (2002) J Electroceram 8:107. doi:10.1023/A:1020599728432
7. Srinivasan G, Rasmussen E, Levin B, Hayes R (2002) Phys Rev B 65:134402. doi:10.1103/PhysRevB.65.134402
8. Dong SX, Zhai J, Li JF, Viehland D (2006) J Appl Phys 88:082907
9. Dong SX, Cheng J, Li JF, Viehland D (2003) Appl Phys Lett 83:4812. doi:10.1063/1.1631756
10. Astrov DN, Al'shin BI, Zhorin RV, Drobyshev LA (1968) Sov Phys JETP 28:1123
11. Odell TH (1965) Electron Power 11:266
12. Boomgaard JVD, Born RAJ (1978) J Mater Sci 13:1538. doi:10.1007/BF00553210
13. Boomgaard JVD, Terrell DR, Born RAJ, Giller HFJI (1974) J Mater Sci 9:1705. doi:10.1007/BF00540770
14. Kobayashi KI, Morinaga H, Araki T (1992) J Magn Magn Mater 104–107:413. doi:10.1016/0304-8853(92)90857-K
15. Rahman IZ, Ahmed TT, Powell L (2003) J Met Nano Mater 17:9
16. Kim WC, Kim SJ (2001) IEEE Trans Magn 37:2362. doi:10.1109/20.951173
17. Islam RA, Priya S (2006) J Am Ceram Soc 89(10):3147. doi:10.1111/j.1551-2916.2006.01205.x
18. Cancarevic M, Zinkavich M, Aldinger F (2005) Mater Sci Forum 494:67
19. Ringgaard E, Nielsen ER, Wolny WW (2001) In: Proceedings of 2000 12th IEEE internationl symposium on application of ferroelectrics, vol 1, p 451
20. Cerovic D, Momcilovic I, Kiss SJ (1972) J Mater Sci 7:735. doi:10.1007/BF00549901
21. Shrotri JJ, Kulkarni SD, Despande CE (1999) J Mater Chem Phys 59:1. doi:10.1016/S0254-0584(99)00019-X
22. Ahmed TT, Rahman IZ, Rahman MA (2004) J Mater Process Technol 153–154:797
23. Okamura T, Kojima Y (1952) Phys Rev 86(6):1040. doi:10.1103/PhysRev.86.1040.2
24. Newnham RE (1989) Rep Prog Phys 52:123. doi:10.1088/0034-4885/52/2/001